Microengineered biosynthesized cellulose as anti-fibrotic in vivo protection for cardiac implantable electronic devices

Robotti, Francesco ; Sterner, Ita ; Bottan, Simone ; Monné Rodríguez, Josep M ; Pellegrini, Giovanni ; Schmidt, Tanja ; Falk, Volkmar ; Poulikakos, Dimos ; Ferrari, Aldo ; Starck, Christoph

Abstract: Upon cardiac implantable electronic device (CIED) exchange, upgrade, or revision surgery patients are exposed to a considerable risk of adverse events. The presence of firm fibrotic tissue endangers these procedures. Leads can be damaged in the attempt of freeing them from fibrotic tissue. Hematoma can form as result of capsulectomy, pocket debridement and leads dissection. Due to the increasing number of CIED exchange, upgrade and revision surgeries, the incidence of related complications is expected to rise in the near future.The aim of the study was to evaluate the feasibility, safety, and performance of a rationally micro-engineered non-resorbable biosynthesized cellulose (BC) membrane as conformal wrapping protection around CIED implants. Protective membranes were generated by means of a recently established method to transfer on-demand microscale geometries onto the surface of BC. A chronic minipig animal model was selected to investigate the performance of the BC anti-fibrotic protection, directly measured as reduction of fibrotic tissue formation. Sixteen (n = 16) animals received each one BC coated pacemaker (PMC) and one native pacemaker (BI) at equivalent anatomical sites. BC protective layers were juxtaposed around pacemakers through a fast and well-repeatable procedure. Explants were performed at 3 and 12 months after implantation. Endpoint analysis showed that the BC protective layers were 100% integer, with no sign of chemical or mechanical degradation and appeared as a thin layer of white-tan material, adherent to the surrounding thin fibrous capsule, from which it could be peeled off by gently pulling with forceps. The protective effect of micro-engineered BC yielded an average thickness reduction of 66% of the fibrotic tissue thickness generated around PMC, as compared to that measured around the naked counterpart (i.e. the BI). When protected by in BC, both the generator and the proximal parts of the leads were completely free from fibrotic tissue. The insertion of an anti-adhesive, non-resorbable and well-tolerated BC interface between the implant and the surrounding tissue in the surgical pocket significantly reduced the formation of fibrotic tissue, ensuring an easy access to the device pocket, and thus creating the conditions for simplified CIED revision surgeries.

DOI: https://doi.org/10.1016/j.biomaterials.2019.119583

Originally published at:
Robotti, Francesco; Sterner, Ita; Bottan, Simone; Monné Rodríguez, Josep M; Pellegrini, Giovanni; Schmidt, Tanja; Falk, Volkmar; Poulikakos, Dimos; Ferrari, Aldo; Starck, Christoph (2020). Micro-engineered biosynthesized cellulose as anti-fibrotic in vivo protection for cardiac implantable electronic devices. Biomaterials, 229:119583.
DOI: https://doi.org/10.1016/j.biomaterials.2019.119583

Biomaterials 229 (2020) 119583

Contents lists available at ScienceDirect

Biomaterials

journal homepage: www.elsevier.com/locate/biomaterials

Microengineered biosynthesized cellulose as anti-fibrotic *in vivo* protection for cardiac implantable electronic devices

Francesco Robotti[a,c,1], Ita Sterner[b,1], Simone Bottan[c], Josep M. Monné Rodríguez[d,**], Giovanni Pellegrini[d], Tanja Schmidt[e], Volkmar Falk[b,f,g,h], Dimos Poulikakos[a], Aldo Ferrari[a,i,*], Christoph Starck[b,g,***]

[a] Laboratory of Thermodynamics in Emerging Technologies, Department of Mechanical and Process Engineering, ETH Zurich, Sonneggstrasse 3, CH-8092 Zurich, Switzerland
[b] Department of Cardiothoracic and Vascular Surgery, German Heart Center Berlin, Berlin, Germany
[c] Wyss Zurich Translational Center, Zurich, Switzerland
[d] Laboratory for Animal Model Pathology, Institute of Veterinary Pathology, Vetsuisse Faculty, University of Zurich, Zurich, Switzerland
[e] Charité- Universitätsmedizin Berlin, Forschungseinrichtungen für experimentelle Medizin, Berlin, Germany
[f] Division of Cardiovascular Surgery, Charité, Berlin, Germany
[g] German Center of Cardiovascular Research (DZHK), partner site, Berlin, Germany
[h] Department of Health Science and Technology, ETH Zurich, Switzerland
[i] EMPA, Swiss Federal Laboratories for Material Science and Technology, Überlandstrasse 129, Dübendorf 8600, Switzerland

ARTICLE INFO

Keywords:
Foreign body reaction
Fibrosis
CIED exchange
Cellulose
Topography
Animal experiments
Pacemaker

ABSTRACT

Upon cardiac implantable electronic device (CIED) exchange, upgrade, or revision surgery patients are exposed to a considerable risk of adverse events. The presence of firm fibrotic tissue endangers these procedures. Leads can be damaged in the attempt of freeing them from fibrotic tissue. Hematoma can form as result of capsulectomy, pocket debridement and leads dissection. Due to the increasing number of CIED exchange, upgrade and revision surgeries, the incidence of related complications is expected to rise in the near future.The aim of the study was to evaluate the feasibility, safety, and performance of a rationally micro-engineered non-resorbable biosynthesized cellulose (BC) membrane as conformal wrapping protection around CIED implants. Protective membranes were generated by means of a recently established method to transfer on-demand microscale geometries onto the surface of BC. A chronic minipig animal model was selected to investigate the performance of the BC anti-fibrotic protection, directly measured as reduction of fibrotic tissue formation. Sixteen (n = 16) animals received each one BC coated pacemaker (PMC) and one native pacemaker (BI) at equivalent anatomical sites. BC protective layers were juxtaposed around pacemakers through a fast and well-repeatable procedure. Explants were performed at 3 and 12 months after implantation. Endpoint analysis showed that the BC protective layers were 100% integer, with no sign of chemical or mechanical degradation and appeared as a thin layer of white-tan material, adherent to the surrounding thin fibrous capsule, from which it could be peeled off by gently pulling with forceps. The protective effect of micro-engineered BC yielded an average thickness reduction of 66% of the fibrotic tissue thickness generated around PMC, as compared to that measured around the naked counterpart (i.e. the BI). When protected by in BC, both the generator and the proximal parts of the leads were completely free from fibrotic tissue. The insertion of an anti-adhesive, non-resorbable and well-tolerated BC interface between the implant and the surrounding tissue in the surgical pocket significantly reduced the formation of fibrotic tissue, ensuring an easy access to the device pocket, and thus creating the conditions for simplified CIED revision surgeries.

* Corresponding author. Laboratory of Thermodynamics in Emerging Technologies, Department of Mechanical and Process Engineering, ETH Zurich, Sonneggstrasse 3, CH-8092 Zurich, Switzerland.
** Corresponding author.
*** Corresponding author. Department of Cardiothoracic and Vascular Surgery, German Heart Institute Berlin Augustenburger Platz 1, 13353, BerlinGermany.
E-mail addresses: josep.monnerodriguez@uzh.ch (J.M. Monné Rodríguez), aldo.ferrari@ltnt.iet.mavt.ethz.ch (A. Ferrari), starck@dhzb.de (C. Starck).
[1] Equal contribution.

https://doi.org/10.1016/j.biomaterials.2019.119583
Received 21 May 2019; Received in revised form 21 October 2019; Accepted 26 October 2019
Available online 31 October 2019

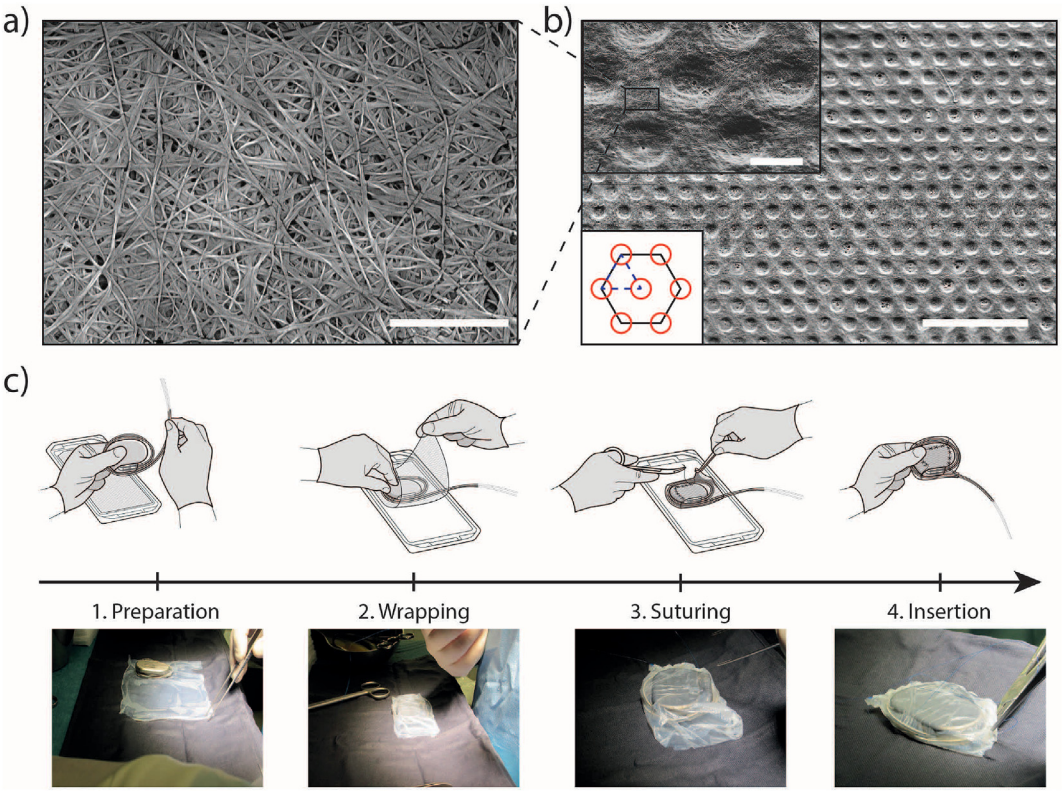

Fig. 1. SEM imaging of implanted micro-structured bio-synthetized cellulose (BC) and surgical procedure used to test the BC coating membrane: a) Fibrous structure of BC. Scale bar 2 μm. b) Micro-well pattern on BC surface. Representative area homogeneously structured. Top-right inset detail of the micro-wells, where the fibrous structure of the material is evident. Bottom-left inset top-view schematic of the layout of the micro wells on the surface. Red circles represent the micro-wells, solid black line depicts the hexagonal arrangement of the features and the blue dashed line highlights the elemental cell shaped as an equilateral triangle with 10 μm side length. Scale bar 300 μm. Scale bar in the inset 5 μm. c) Graphic flowchart of the entire surgical procedure. (For interpretation of the references to colour in this figure legend, the reader is referred to the Web version of this article.)

1. Introduction

The annual number of cardiac implantable electronic device (CIED) implantations has nearly doubled in the last 15 years, to about 2 million devices implanted annually worldwide [1]. The growth is explained by the introduction of cardiac resynchronization therapy and an increased use of implantable cardioverter defibrillators (ICDs) [2,3]. In the frame of an ageing Western population, these figures are bound to further rise [4].

Despite the high functional performance of current CIEDs, important drawbacks are connected to their implantation. Lead related complications account for approximately 30% of all adverse events recorded within 6 months after implantation [5]. Problems at the generator pocket (e.g. lead damage, pocket hematoma), although underrepresented in scientific literature, occur with similar incidence [5]. Risks related to generator replacement procedures are frequently underestimated. In this direction, a recent prospective multicentre study has clearly demonstrated that device replacement is associated with a considerable threat of major and minor adverse events [6].

A common source of complications is fibrotic adhesion, generated in and around the surgical pocket as a result of foreign body reaction [7,8]. The sequence of events leading to the deposition of fibrotic tissue starts immediately after device implantation, and is sustained over weeks to months by the engagement and activation of fibroinflammatory cell mediators and actuators [9]. Upon revision surgery, the necessity to free the device as well as the leads from the embedding tissue exposes to the risk of lead damage and in such cases escalating the procedure to a full lead revision surgery [10]. In addition, a thick fibrotic tissue may negatively influence the conditions for the onset of local infections, enforcing a barrier with low vascularization and poorly conducive to circulating immune cells. This renders infections at the implant interface significantly more likely during the generator exchange, device upgrade or revision procedures [11] than upon *de novo* implantations [12]. In this scenario, a healthy regeneration of the tissues lining the surgical pocket is essential to lower the risk of such procedures and/or revision and avoid pocket infections. A universal solution to this problem is still missing, representing an unmet clinical need connected to CIED implantation procedures.

Bacterial cellulose (BC) has emerged as a well-tolerated and stable hydrogel material for biomedical applications [13,14]. The strong hydrophilicity of cellulose nanofibers confers antifouling properties to the surface of BC layers [15]. In addition, the interaction with human cells is modulated by the implementation of optimized microscale topographies [16,17].

Much information regarding the biological effect of rationally-developed surface geometries has been reported for implant materials of different nature, including metals, elastomers, plastic polymers and others [18–20]. In general, topographic features with lateral and vertical size of few microns are able to physically interfere with the establishment and maturation of integrin contacts, thereby promoting or demoting cell adhesion, migration and differentiation [21,22]. While anisotropic textures, in the form of gratings, facilitate cell spreading and polarization [23] symmetric arrays of isotropic features have the opposite effect, bestowing anti-adhesive properties to the target substrate [24].

Surface geometries are introduced on BC by a lithographic protocol harnessing the fermentation process [25]. Specifically, symmetric arrays of hexagonal pits in the micron range interfere with the adhesion of cells involved in foreign body reaction, including fibroblasts and macrophages [24]. A parametric optimization of the pit dimensions and

spatial arrangement renders BC substrates that significantly hamper the adhesion and differentiation of the cellular mediators and actuators of fibrosis [24].

In the present study, we describe the design, development and *in vivo* translation of a surface-engineered BC membrane representing an anti-fibrotic protection at the interface between CIED devices and the surgical pocket. The application of this new medical device reduced significantly the formation of fibrotic tissue in a large, and clinically relevant animal (minipig) model over a period of 3 and 12 months. The long-term analysis provides evidence of BC *in vivo* stability and safety upon implantation. The anti-fibrotic effect is demonstrated in comparison with identical procedures of bare implant (BI) deployment. Non-invasive measurements are presented to showcase the material stability and exclude interference with the electric function of implanted CIED devices. Altogether, these results provide the validation of a resolutive anti-fibrotic protection, supporting its translation to the clinical application.

2. Results

2.1. Fabrication, handling and usability of antifibrotic BC membranes

Anti-fibrotic membranes comprising surface microstructured BC were generated by guided assembly biolithography (GAB [25]) using an elastomeric mold to transfer a triangular array of hexagonal wells (Fig. 1). Specifically, the topographical features were selected to minimize the adhesion and differentiation of the cellular mediators and effects of foreign body reaction, i.e. monocytes and fibroblasts; respectively [24]. The quality of lithographic transfer and the overall nano- and microtopography were characterized by SEM imaging (Fig. 1a–b). Macroscopically, individual BC membranes measured 10 × 20 cm, showed excellent conformability (Supplementary Fig. 1) and tensile strength (1.6 ± 0.3 N; Supplementary Fig. 2), which were overall compatible with the suturing process.

Towards the application of the BC membranes as anti-fibrotic protection surrounding BI, the typical volume increment caused by the cloaking layer was evaluated. Specifically, the additional hindrance was in the range of 5 ml, therefore representing less than 7% of the overall target implant volume. Consistently, the application of the BC layer did not require a larger incision or the creation of a bigger pocket and did not introduce any significant modification of the standard surgical routine (Supplementary Fig. 3).

Another important aspect consisted in the time to apply the BC layer, which included an initial wrapping followed by suturing with a monofilament non-resorbable Prolene suture (Fig. 1c). In general, wrapping of the BI was reproducible (Fig. 1c and d). The surgical procedure was completed in 46 ± 19 min, as compared to 42 ± 20 min in the control case of BI implantation without the BC membrane. The increment in procedural time was not statistically significant.

2.2. Surgery and post-surgical observations

Two groups of 8 adult female minipigs (*Aachener minipigs*) entered the study. A complete parametric description of the animals is reported in the materials and methods. Each experimental animal received two PMs, which were implanted at axisymmetric locations of the neck, as reported in Fig. 2. In particular, a reference implant was deployed as for the standard of care, i.e. without antifibrotic protection (hereafter identified as BI). The counterpart was wrapped with the anti-fibrotic BC membrane (hereafter identified as PMC; Fig. 1). In this case, both the device case and a proximal segment of the leads were included in the BC wrapping (Fig. 1c). For both implants, the distal part of the leads was transvenously implanted in the right atrium in a regular fashion and the device was programmed to an atrial sensing mode (OAO).

The two animal groups were sacrificed at 3 and 12 months after implantation; respectively. No animal required special treatment of the surgical wound or revision surgeries of the implantation sites. All wounds healed without any complication. Taken together, after 3- and 12-months BC coated implants did not exhibit signs of infection or, more in general, suboptimal surgical result. During husbandry, one animal (included in the 12 months group) exhibited signs of back pain and persistent lameness. It was therefore sacrificed before due time; i.e. at 4 months post implantation. None of the other animals showed fever or dysfunction, distress, disability or disorder indicating changes in general body condition or a systemic inflammatory reaction throughout the whole duration of the study (blood testing, data not shown).

Three independent approaches were adopted to gather non-invasive measurements of the BC membrane performance. First, ultrasound images were obtained using a high-resolution FUJIFILM Vevo 3100 ultrasound-imaging machine (18–22.5 MHz transducers) to assess the stability and conformity of the BC protection. At each time of measure (3 and 12 months) the presence of a continuous BC membrane around the implant was monitored. Specifically, BC appeared as a dark layer juxtaposed to the implant. A qualitative evaluation of the tissue build-up at the external surface of the BC membrane was performed (Fig. 2b). Second, a computer tomography CT-scan was performed on the day of the explant. The resulting 3D reconstruction (Fig. 2c) was used to exclude implant migration and erosion of the surrounding tissues. Finally, the electric activity of each PMC was detected and evaluated in comparison to the BI counterpart. Values of p-wave, voltage threshold and impedance were registered to evaluate possible detrimental effects of cellulose wrapping on the electric functionality of the devices and are reported in Table 1. No significant variations in the device electric function were detected.

2.3. Macroscopic observations

At the time of explant, all animals from both groups showed clean surgical sutures with no sign of dehiscence and/or infection. A capsule comprising a light beige, firm fibrous tissue that anchored the devices (Fig. 3a and b) surrounded all implants (i.e. BI and PMC). In all surgical pockets, the fibrous capsule was intact with no sign of tearing and/or disruption. The regional lymph nodes were macroscopically unremarkable in both post-implantation groups.

Three-month post-implantation group. The inner surface of the BI capsule (facing the implant) appeared smooth and well separated from the header of the underlying devices (Fig. 3c). Less than 0.5 ml of clear fluid was recovered from the device pocket hosting BI of all animals. The BI leads, including the end of the electrodes, were embedded in a markedly thick and firm fibrous connective tissue, which hampered their release (Fig. 3c). Therefore, in all animals, dissection or even severing of the leads in multiples locations was necessary for release. On the other hand, all animals with PMC showed intact cellulose with no signs of degradation and/or disruption. BC appeared as a thin layer of white-tan material with a slightly granular surface, adhered to the surrounding fibrous capsule, from which it could be easily peeled by pulling with forceps (Fig. 3f). The leads confined within the BC pocket were free from connective tissue and could be easily removed from the pocket in their native configuration.

Twelve-month post-implantation group. The fibrotic capsule around BI showed a macroscopic morphology similar to that described at 3 months. The leads strongly adhered to the capsule through a firm and thick fibrous proliferation. Dissection or even severing of the leads was necessary to extract the devices from the pocket (Fig. 3d). One BI capsule (minipig 9) exhibited small amounts of fibrin adhered to the inner surface and four BI capsules (minipigs 12, 13, 14, and 15) exhibited small multifocal areas of red/brown discolouration interpreted as hemorrhages (Fig. 3d). On the other hand, all PMC pockets showed intact BC with no signs of degradation and/or disruption. As described at 3 months, BC appeared as a thin layer of white-tan material that could be easily separated from the surrounding capsule (Fig. 3e).

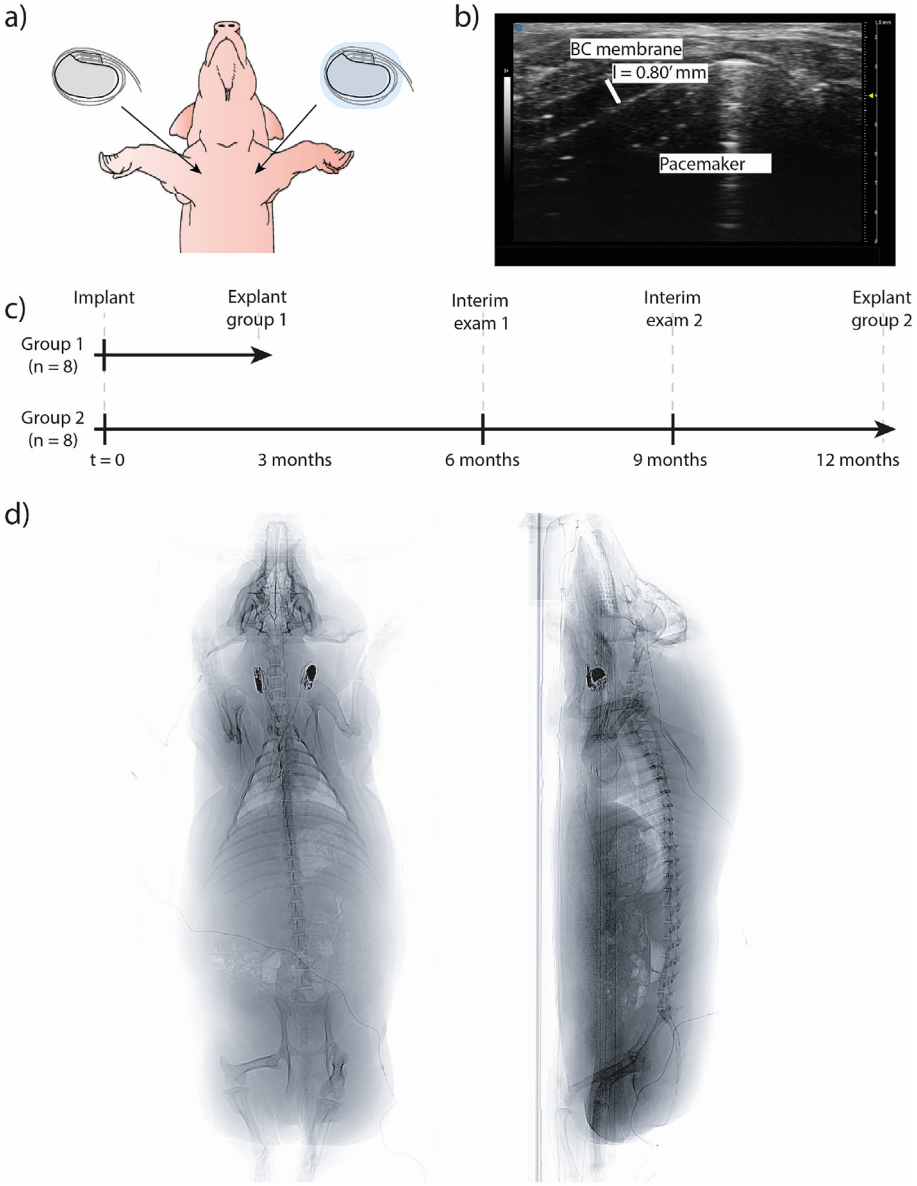

Fig. 2. Study schedule and summary of *in vivo* exams. a) schematic of the implant layout. b) High-resolution ultrasound imaging of the pacemaker covered by the cellulose membrane. c) Schedule of the study with intermediate and final follow up for the two study groups (group 1 and group 2, 3 and 12 months follow up, respectively). d) CT scan of a minipig showing the positioning of the pacemakers at the 12-month follow-up.

Table 1
Electric parameters of implanted pacemakers.

Animal	PMC			BI		
	p-Wave (mV)	Threshold @ 0.4 s (V)	Impedance (Ω)	p-Wave (mV)	Threshold @ 0.4 s (V)	Impedance (Ω)
1	2.8–4.0	1.75	794	0.5–0.7	0.75	427
2	4.0–5.66	2.0	130	> 5.6	0.75	177
3	4.0–5.6	0.75	567	2.8–4.0	1	767
4	> 5.6	1.25	635	2.8–4.0	1	590
5	> 5.6	0.75	519	1.4–2.0	1.25	468
6	2.0–2.8	0.5	520	> 5.6	0.25	510
7	> 5.6	0.75	480	> 5.6	0.75	542
8	1.4–2.0	1.5	478	> 5.6	1.25	703
9	> 5.6	–	470	0.7–1.0	–	470
10	0.7–1.0	–	458	2.0–2.8	–	634
11	4–5.6	0.75	426	> 5.6	0.5	501
12	4–5.6	0.75	550	> 5.6	0.5	475
13	2.8	1.5	567	4.0	1.0	450
14	1.3	0.75	646	3.1	0.75	589
15	2.8	1.25	754	2.8	1.0	769

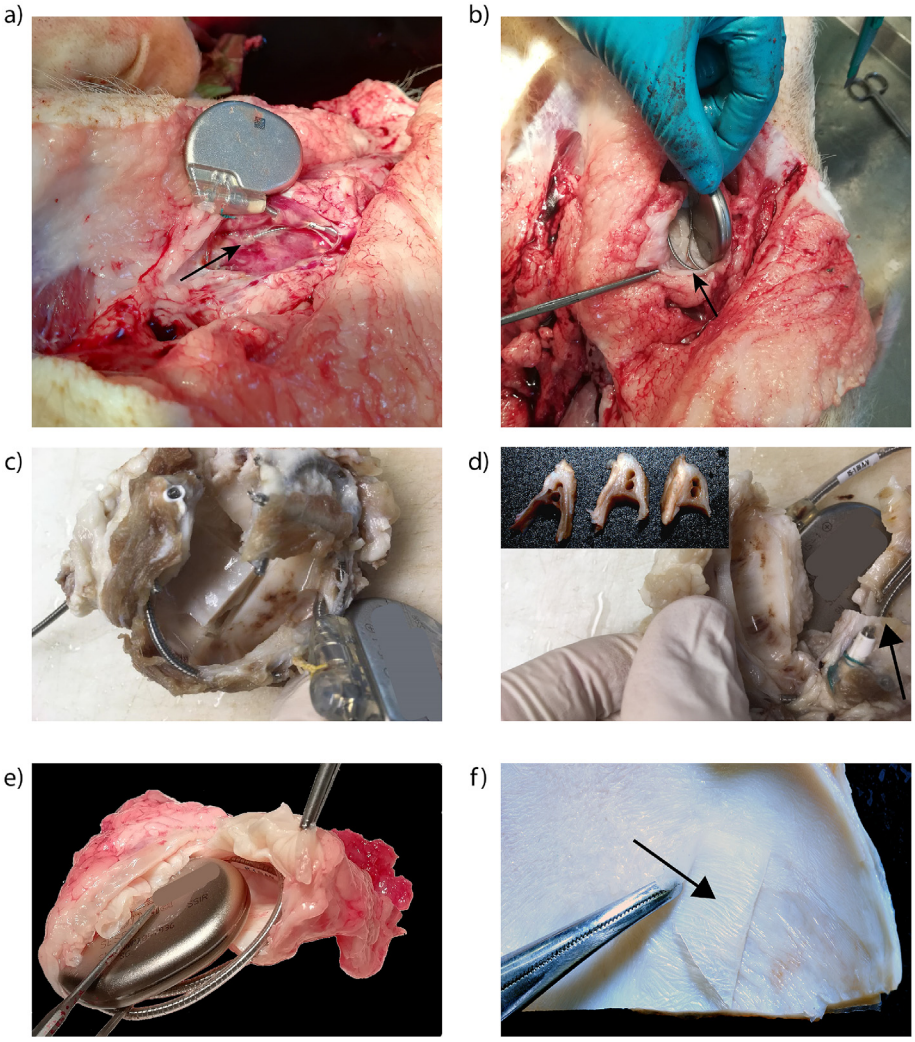

Fig. 3. Gross observations associated with PMs and PMCs. a) View of the BI fibrotic capsule upon removal (3-month group). BI leads are clearly trapped in thick fibrotic tissue (arrow) b) View of the PMC fibrotic capsule upon removal (3-month group). PMC leads are clearly free of tissue (arrow) and the cellulose membrane appears clear and intact. c) Inner view of a BI pocket containing the device. The leads are firmly surrounded by thick fibrous connective tissue (arrow). d) Inner surface of 12-month BI capsule without the device. The inner capsular surface shows multifocal hemorrhages (arrowhead). The leads were severed in order to be released from the surrounding fibrotic capsule (arrows). The inset shows the tracks created by the leads after removal. e) View of an opened 12-month PMC capsule. The device and the leads can be easily removed by pulling out with forceps. f) The picture shows how the BC can be easily pulled out with forceps from the surrounding fibrotic capsule.

Proximal leads confined within the BC pocket were not surrounded by connective tissue and could be easily removed from the pocket (Fig. 3e). A small amount of turbid fluid (< 1 ml) was detected within the PMC device pocket of one animal (minipig 13) and another animal exhibited small strands of fibrin adhered to the device surface (minipig 14). Two animals (minipigs 9 and 14) exhibited small foci of white discoloration at the inner surface of BC (interpreted as mineralization in the histological examination; Supplementary Fig. 4).

2.4. Histopathological observations

The biological response to the BI and PMC devices was defined by the development of a moderately thick, well-vascularized fibrotic capsule surrounding the BI body and the leads. The results of the semi-quantitative histological assessment are summarized in Table 2.

Three months post implantation. All animals developed a fibrotic capsule around the medical devices accompanied by a chronic inflammatory response (foreign body reaction). The fibrotic tissue comprised reactive fibroblasts (showing plump nuclei) in a collagenous stroma with moderate numbers of small calibre blood vessels (i.e. neoangiogenesis, Fig. 4a and b). Van Gieson's staining (VG) showed higher amount of mature collagen fibres (stained in red) in the outer layers of the fibrotic capsule compared to the mid to inner layers (stained as yellow), which indicates the different stages of maturation of the fibrotic capsule (Supplementary Fig. 5). The fibrotic reaction compressed, infiltrated and replaced the neighbouring tissues, including adipose tissue, muscle and salivary glands, which showed signs of severe degeneration. The nature of the inflammatory response was similar in BIs and PMCs, being dominated in both implant types by macrophages (Iba-1+; Fig. 5a and b), moderate numbers of T-lymphocytes ($CD3^+$; Fig. 5c and d) and occasional B-lymphocytes ($CD20^+$; Fig. 5e and f) and plasma cells. Polymorphonuclear cells, including eosinophils, neutrophils as well as aggregates of multinucleated giant cells (Iba-1+) were less represented. The macrophage infiltrates were diffusely observed throughout the capsule and often showed higher numbers in the inner regions of the capsule (close to the CIED and cellulose) or around perivascular regions. Multinucleated giant cells tended to form aggregates in the outer region of the capsule and rarely infiltrated the inner surface (Fig. 4d). Individual T-lymphocytes were diffusely observed throughout the capsule or sometimes forming small perivascular aggregates. In both groups, moderate numbers of blood vessels ($CD31^+$ positive endothelial cells; inset of Fig. 4e) were identified throughout the capsule. Areas with higher amount of collagen tend to show reduced numbers of blood vessels, on the other hand, higher numbers of small *de novo* generated blood vessels were found in association with inflammatory infiltrates, particularly in regions close to the inner surface of the capsule (Fig. 4e).

The interface with the device exhibited significant differences between BI and PMC. First, BIs fibrotic capsules often showed round to elongated cells palisading along the surface. This configuration is reminiscent of synovial metaplasia (Fig. 4e), frequently reported as a feature of the reaction to silicone breast and joint prostheses [26]. PMC did not show histological traits compatible with synovial metaplasia. A subset of PMCs (2/8) cases showed fibrin deposition on the surface of

Table 2
Biocompatibility of micro-structured BC. Semi – quantitative scoring of main indicators of immune reaction. Subtotal and total scores considering the following histological features: number of fibroblasts, number of inflammatory cells, multinucleated giant cells, fibrin deposition, synovial metaplasia, neovascularization, hemorrhages, capsular erosion and haemosiderin. BI = native pacemaker; PMC = BC coated pacemaker; D = dorsal region; V = ventral region.

3-month group																												
Animal	**1**				**2**				**3**				**4**				**5**				**6**				**7**				**8**			
Implant	**BI**		**PMC**		BI		PMC		**BI**		**PMC**		**BI**		**PMC**		**BI**		**PMC**		**BI**		**PMC**		**BI**		**PMC**		**BI**		**PMC**	
Location	**D**	**V**	**D**	**V**	D	V	D	V	**D**	**V**	**D**	**V**	**D**	**V**	**D**	**V**	**D**	**V**	**D**	**V**	**D**	**V**	**D**	**V**	**D**	**V**	**D**	**V**	**D**	**V**	**D**	**V**
Subtotal Score	15	16	7	8	10	8	4	6	12	3	7	9	9	7	5	7	11	12	6	7	9	7	7	8	12	10	5	6	6	7	5	5
Total Score	15.5		7.5		9		5		7.5		8		8		6		11.5		6.5		8		7.5		11		5.5		6.5		5	
12-month group																																
Animal	**9**				**10**				**11**				**12**				**13**				**14**				**15**				**16**			
Implant	**BI**		**PMC**		BI		PMC		**BI**		**PMC**		**BI**		**PMC**		**BI**		**PMC**		**BI**		**PMC**		**BI**		**PMC**		**BI**		**PMC**	
Location	**D**	**V**	**D**	**V**	D	V	D	V	**D**	**V**	**D**	**V**	**D**	**V**	**D**	**V**	**D**	**V**	**D**	**V**	**D**	**V**	**D**	**V**	**D**	**V**	**D**	**V**	**D**	**V**	**D**	**V**
Subtotal Score	9	9	4	4	6	6	4	3	6	6	2	5	4	5	2	2	6	6	2	3	2	3	2	2	2	2	2	2	–	–	–	–
Total Score	9		4		6		3.5		6		3.5		4.5		2		6		2.5		2.5		2		2		2		–		–	

the cellulose. Second, small multifocal erosions of the superficial capsule associated with necrotic debris, fibrin, and sometimes hemorrhages were present in all BIs but only in one of the 8 PMC (Fig. 4f). Third, multifocal hemorrhages were more common in BI (7/8) than PMC (4/8, Fig. 4f). Fourth, multifocal regions of fibroblasts haphazardly arranged in bundles were observed (3/8) in correspondence of BIs, but not in the PMC counterparts (Fig. 4c). Fifth, most BI (5/8) showed macrophages containing intracytoplasmic golden/brown material interpreted as haemosiderin, not observed in PMC. Finally, one BI showed a focal area of mild mineralization.

Twelve months post-implantation. The fibrotic capsule around BIs was thicker than at 3 months (Fig. 6, Fig. 8). This increase in thickness was associated with higher amount of mature collagenous bands (stained in red with VG stain; Supplementary Fig. 5) than the 3 month fibrotic capsule and the maturation gradient (outer layers more mature than inner layers) was more conspicuous. Areas showing a denser collagenous matrix where characterized by a reduced number of fibroblasts with no signs of cellular activation (i.e. plump nuclei). As at 3 months, BIs exhibited regions (3/7) with irregularly arranged interwoven bundles of fibroblasts (Fig. 6c).

Like in the 3-month group, the inflammatory response was dominated by macrophages, with moderate T-lymphocytes and occasional B-lymphocytes, plasma cells and rare polymorphonuclear. The number of macrophages (Fig. 7a and b) and T-lymphocytes (Fig. 7c and d) was moderately reduced compared to the 3 month group, in particular in those areas where the fibrotic capsule showed higher maturation with

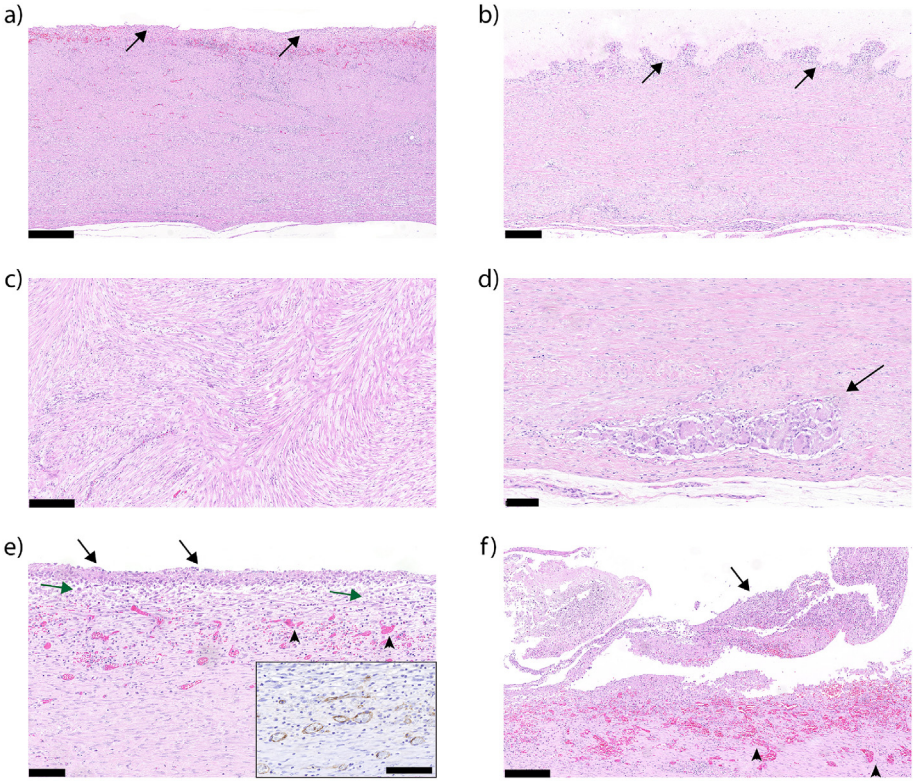

Fig. 4. Histopathological observations at 3 months follow up. a) Sub gross view of the BI capsule (arrows indicate inner surface of the capsule). Scale bar: 500 μm. b) Sub gross view of the PMC fibrotic capsule with the cellulose (arrows). Scale bar: 250 μm. c) Close up view of the BI fibrotic capsule showing fibroblasts irregularly arranged in bundles. Scale bar: 250 μm. d) Close up view of a foci of multinucleated giant cells in a PMC fibrotic capsule. Scale bar: 100 μm. e) Close up view of the inner BI fibrotic capsule with superficial synovial metaplasia (black arrows), superficial inflammation (green arrows) and neovascularization (arrowheads). Scale bar: 100 μm. Inset: CD31 staining to reveal neovascularization. Scale bar: 100 μm. f) Close up view of the superficial BI capsule with a focal erosion associated with fibrin deposition hemorrhages and inflammation (arrow), and areas neovascularization (arrow heads). Scale bar: 250 μm. (For interpretation of the references to colour in this figure legend, the reader is referred to the Web version of this article.)

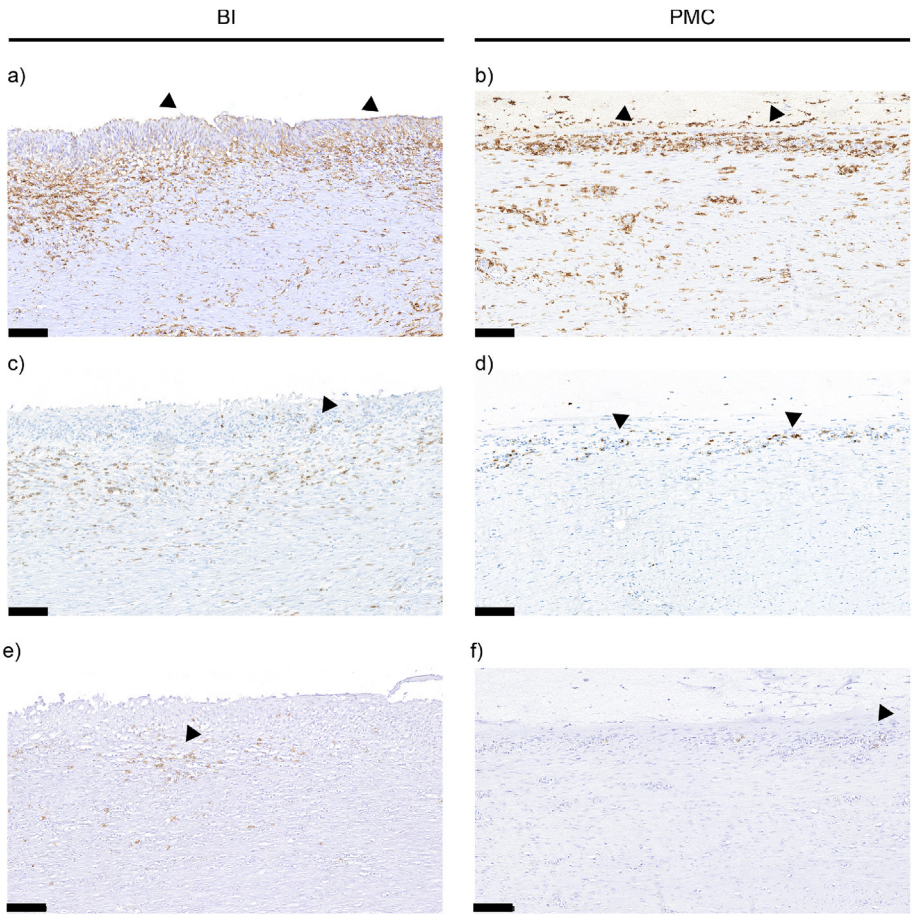

Fig. 5. Immunohistochemical examination at 3-month post implantation of BI (left panel) and PMC (right panel). A and B) Iba-1 antibody shows numerous macrophages diffusely infiltrating the inner layers of the fibrotic capsule. The BI capsular surface in contact with the medical device exhibits synovial metaplasia with small to moderate numbers Iba-1 positive cells (arrows, A). The PMC capsular surface in contact with the cellulose shows a thin rim of infiltrating macrophages (arrows, B). C and D) CD3 antibody shows small to moderate numbers of T-lymphocytes diffusely infiltrating the inner layers of the fibrotic capsule including small numbers in the BI synovial metaplasia (arrows, C) and a small rim of positive cells along the PMC capsular surface in contact with the cellulose (arrows, D). E and F) CD20 antibody shows small numbers of B-lymphocytes diffusely scattered throughout the inner layers of the fibrotic capsule of BI (arrow, E) and PMC (arrow, F). Scale bar: 100 μm.

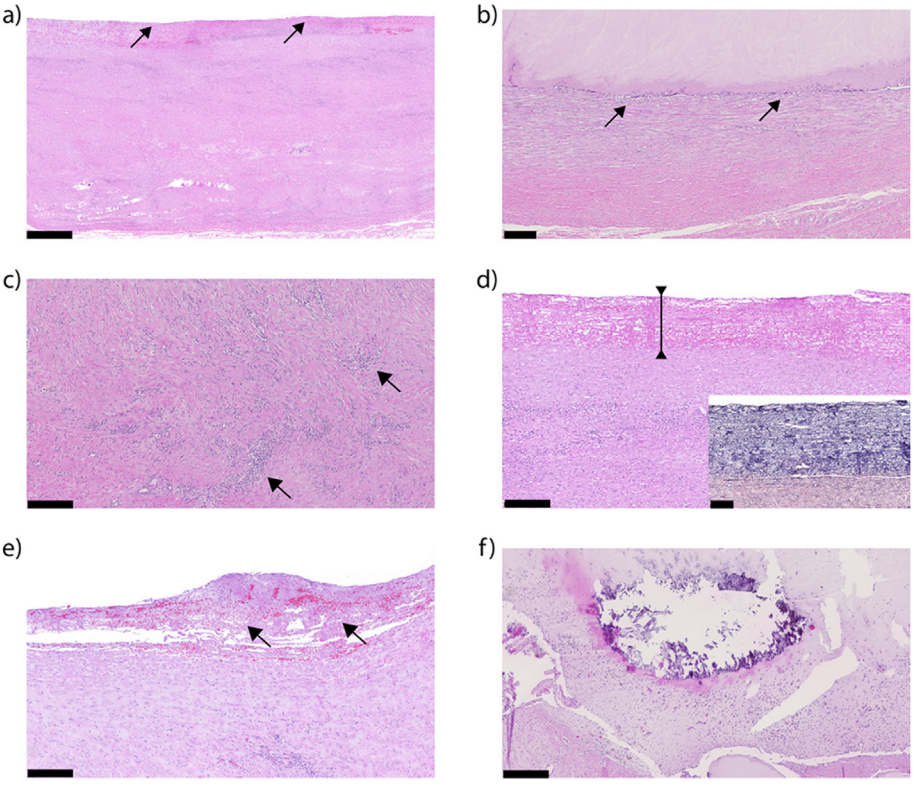

Fig. 6. Histopathological observations at 12 months follow up. a) Sub gross view of the BI capsule (arrows indicate inner surface of the capsule). Scale bar: 1 mm. b) Sub gross view of the PMC fibrotic capsule with the cellulose (arrows). Scale bar: 250 μm. c) Close up view of a BI fibrotic capsule with multifocal to coalescing foci of inflammation (arrows) and fibroblasts irregularly arranged in bundles. d) Close up view of the inner BI fibrotic capsule with large amount of fibrin deposition. Scale bar: 250 μm Inset: PTAH staining to reveal fibrin. Scale bar: 100 μm. e) Close up view of the superficial BI capsule with a focal erosion associated with fibrin deposition and hemorrhages (arrows). Scale bar: 250 μm. f) Close op view of a calcified focus in the cellulose in contact with the fibrotic capsule. Scale bar: 250 μm.

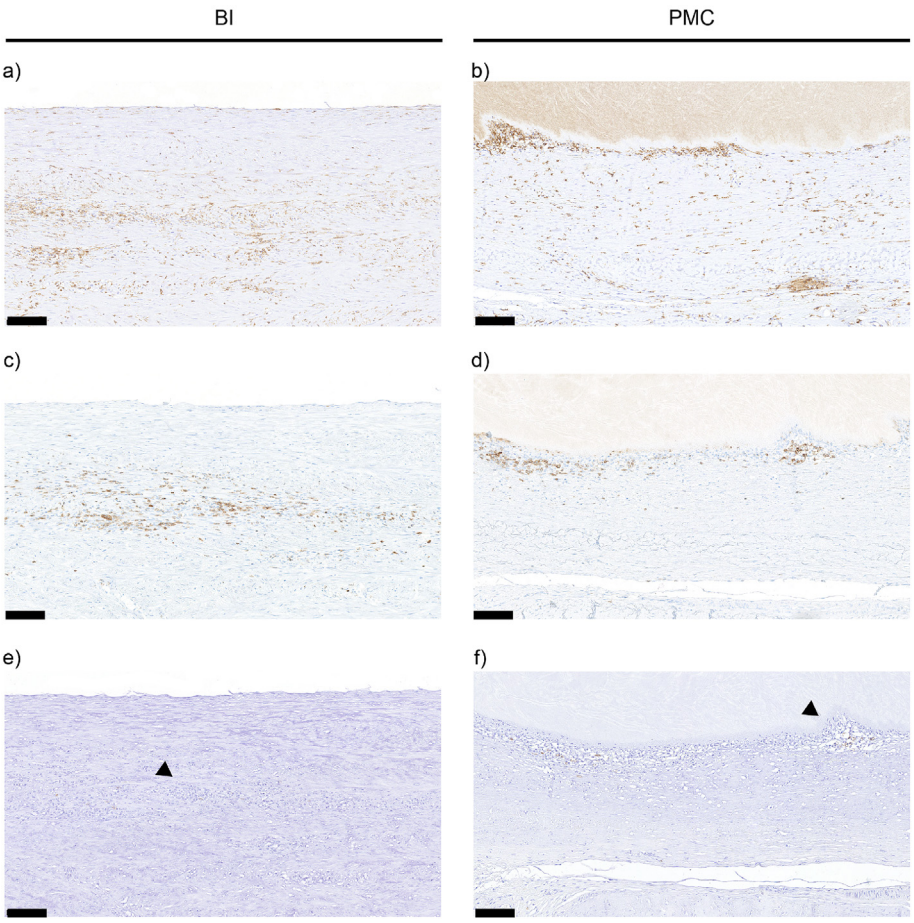

Fig. 7. Immunohistochemical examination at 12-month post implantation of BI (left panel) and PMC (right panel). A and B) Iba-1 antibody shows moderate macrophages diffusely infiltrating the inner layers of the BI (A) and PMC fibrotic capsule (B) C and D) CD3 antibody shows small to moderate numbers of T-lymphocytes diffusely infiltrating the inner layers of the BI (C) and PMC fibrotic capsule (D). E and F) CD20 antibody shows occasional B-lymphocytes diffusely scattered throughout the inner layers of the fibrotic capsule of BI (arrow, E) and PMC (arrow, F). Scale bar: 100 μm.

abundant collagenous deposition. Moreover, at this later time point, multinucleated giant cells were markedly less numerous than at the 3 months, with only one PMC animal showing small groups. Synovial metaplasia and fibrin deposition (Fig. 6d) were detected around BIs (2/7 and 5/7; respectively). Similarly to the 3-month group, moderate numbers of blood vessels were observed throughout the capsule with lower density in collagen dominated areas and higher density in reactive/inflamed areas often close to the inner surface. The band of fibrin deposited at the capsular surface was significantly thicker than at 3 months (Fig. 6d). Superficial capsule erosion was observed both in BIs (2/7) and PMC (1/7; Fig. 6e) as well as tissue mineralization (1/7 BIs and 2/7 PMC; respectively). Mineralization was more prominent in PMCs where it affected the outer BC layer (in contact with the fibrotic capsule). The reaction was characterized by deposition of hyperbasophylic crystalloid to granular material. It did not extend throughout the entire BC layer and did not compromise the membrane integrity (Fig. 6f).

2.5. Quantitative evaluation of fibrotic tissue build-up

Each of the explanted tissue section containing the devices was processed as described in detail in Materials and Methods section with the aim of assessing the thickness of the layer of newly formed fibrotic tissue (Fig. 8a and b), the markers of foreign body reaction and ongoing inflammation. The fibrotic capsule thickness was significantly smaller around PMCs at 3 months compared to BI (0.87 ± 0.28 mm vs. 1.60 ± 0.44 mm; $p < 0.05$, 38% average reduction). At 12 months this difference further increased (0.98 ± 0.43 mm vs. 2.89 ± 0.90 mm; $p < 0.001$, 66% average reduction). The BI capsule was on average in the range of few millimetres, indicating a prompt and continuous response of the animals to the implantation of the devices. The formation of fibrotic tissue in the pocket was significantly reduced in the presence of BC membranes, with an average thickness reduction of 66% (Fig. 8c). Interestingly, the maximum reduction achieved was approximately 80% and occurred in animals showing the highest values of thickness around BI implant.

3. Discussion

Rising incidence of CIED implantation combined with increased life expectancy yields higher implant prevalence, which is associated with a higher burden of device replacement and upgrade/revision surgery [27]. The number of generator exchange and upgrade procedures can be expected to rise. Therefore, the recommendation for lifelong implant must consider - among the risk factors - the hazards related to the replacement of the generator or an upgrade/revision procedure. The mitigation of these risks can follow two different paths: a significant effort has to be made in research and development to extend the longevity of the implantable batteries. Solutions for minimizing complications related to the device pocket must be found [6]. An additional drawback related to re-operation is the significantly higher rate of infection after replacement procedures [28]. Pocket related complication rates after generator exchange or upgrade/revision surgery are considerable [6]. Therefore, every concept simplifying the dissection of device pockets will show a positive effect on complication rates.

The importance of the device pocket as a source of complications is reflected by the clinical introduction of a resorbable, antibacterial envelope (TYRX, Medtronic, USA) to reduce the rate of pocket infections. The results of the WRAP-IT study, a prospective randomized trial on the efficacy of the antibacterial protection, brought further clarification on the beneficial effects of TYRX [29], showing significant reduction of occurrence of infection with the use of the envelope. A different

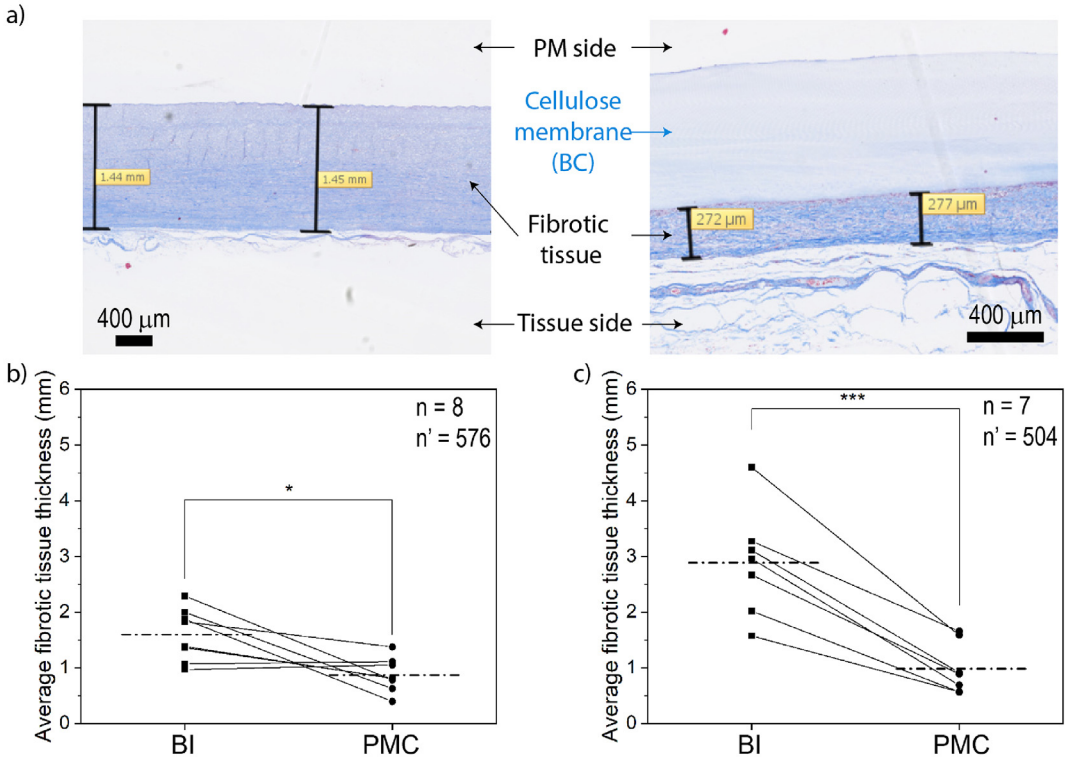

Fig. 8. Histological sampling and thickness measurements: a) Representative sampling for tissue thickness quantification around the BI. b) Quantification and statistical comparison of the measurements of the overall thickness of the fibrotic tissue layer surrounding the BI and PMC at 3 months follow up. c) Quantification and statistical comparison of the measurements of the overall thickness of the fibrotic tissue layer surrounding the BI and PMC at 12 months follow up. The population means are reported as a horizontal dash-dotted line The number of measurements is reported as number n' and the number of independent experiments is reported as the number n. Significant differences between the population means are indicated by asterisks (* for $p < 0.05$ and *** for $p < 0.001$).

approach to CIEDs wrapping is provided by Cangaroo (Azyio Biologics, USA). The Cangaroo envelope is made of decellularized porcine extracellular matrix, which is remodelled by the host into a healthy, vascularized pocket supporting the device and reducing the risk of migration. Up to date, no clinical data are available on the effectiveness of this procedure [30].

Other surgical protocols, including abdominal surgery, similarly adopt adhesion barriers (e.g. Interceed, Seprafilm, etc.) to prevent tissue-to-tissue adhesion upon healing. These gels or films, comprising oxidised regenerated cellulose or hyaluronate carboxymethylcellulose, establish an intervening separation between the operative surfaces within the abdomen [31]. They must be retained until complete healing and eventually reabsorb without inducing foreign body reaction. Compared to the substrate presented in this work, these devices present significant technological differences and a different intended use.

Importantly, neither any of the currently available envelopes for CIEDs nor any of the above-mentioned adhesion barriers specifically targets foreign body response and fibrotic tissue deposition. The approach presented in this work is therefore innovative, as it consists of a non-resorbable material exploiting a new mode of action through the combination of an antifouling material and a rationally developed surface topography.

The insertion of a non-adhesive, non-resorbable and simultaneously well-tolerated interface enables the operator to easily access a clean pocket, simplifying the exchange or upgrade or revision procedure. After the generator pocket is opened in such procedures, there is a frequent need for extensive and time consuming dissection of the leads from fibrotic scar tissue [32], while the tested BC membrane makes this procedure simply unnecessary. The elimination of the need for the lead dissection, reduction of surgical trauma to the pocked and will lead to a relevant decrease of post-operative pocket hematomas. Pocket hematomas are a known risk factor for subsequent pocket infection (Odd Ratio = 8.46 (4.01–17.86)) [33]. Taken together, the easiness of re-operation and the drastically improved accessibility to the site of the implant constitute a parameter of increasing importance in the definition of successful therapeutic strategy.

On the other hand, the quality of the interaction between the implant and the surrounding tissue is what determines the long-term comfort of the patient and contributes to the ultimate success of a surgical procedure comprising a foreign body implant. For numerous implants in soft tissue, foreign body reaction constitutes one of the major causes of discomfort, pain and ultimately revisions [34].

The establishment of a rationally designed, stable interface between the body and the implant is a viable strategy to minimize the complications related to foreign body response. The performance of such a membrane depends on the constitutive properties of the material, in this case BC, and on the capability to specifically tailor the surface topography, an independent physical parameter, in order to elicit specific responses in human cells [21]. In this study, the presence of micro-wells distributed on a hexagonal lattice on a layer of BC aims at the reduction of the adhesion of immune cells and fibroblasts, responsible for the deposition of the new collagen matrix and the creation of the typical dense fibrotic tissue [24]. As reported earlier [24], surface topography proved to successfully influence adhesion of cells *in vitro* and the same effect seems to be reproduced *in vivo*, if quantified through the thickness of the newly deposited tissue. Briefly, the mode of action of such a topography is based on the concept that an isotropic distribution of topographical features on a substrate, on the scale of the cell, creates unfavourable conditions for adhesion.

The thickness of the fibrotic capsule is an important physical parameter to describe the advancement of the foreign body response, but this has to be coupled to biological reporters, especially inflammation markers, to provide a comprehensive description of the *status quo* after 3 and 12 months. Semi-quantitative histological analysis

revealed that the fibroinflammatory reaction elicited by BI and PMCs had comparable morphological features, but with a drastic reduction of the thickness of fibrotic capsules in the latter.

While clearly establishing the stability, safety and performance of the presented micro-engineered BC anti-fibrotic protection, in a clinically relevant large animal model, this study still has limitations. These are of intrinsic nature. Revision and upgrade surgeries are typically performed at > 1 year after the original implant, in humans, which is longer than what could be reproduced in the animal study at hand. Specific traits of inflammatory and foreign body reaction in cardiovascular patients similarly not reproduced in healthful individuals, particularly affecting the extent and nature of fibrotic tissue formation. Altogether, this work provides sufficient *in vivo* evidence for the anti-fibrotic efficacy of a protective layer made of micro-engineered BC, opening to the translation of this innovative medical device.

4. Materials and methods

4.1. Membrane fabrication and surface microstructuring

Surface micro-structured 20 cm × 10 cm biosynthesized cellulose (BC) membrane segments were fabricated using Guided-Assembly Bio-Lithography (GAB), as previously reported [25]. Briefly, cellulose was synthesized by a strain of the bacterium *Acetobacter xylinum* in static culture and with an elastomeric microstructured mold floating at the liquid-air interface. The BC membrane was made of a three-dimensional network of randomly arranged cellulose nanoribbons, resulting in the formation of a multi-layer hydrogel with high porosity (Fig. 1a). Through GAB, the surface of the BC membrane was natively micro-structured with approximately 2 μm deep micro-wells distributed in a centered-hexagonal pattern with characteristic length of 20 μm (Fig. 1b). The diameter of each well was defined as half of the center-to-center distance, namely 10 μm. Importantly, GAB produced a higher degree of order in the nanoscopic arrangement of the ribbons in close proximity of the micro-wells, clearly delineating the surface micro-features [24,25]. The BC membranes were harvested after 1 week of incubation at 27 °C and the bacterial content was removed by 1 M NaOH at 90 °C for 8 h. The pH was finally balanced with a series of washings (≥8 × 1 h washings) in de-ionized (DI) water. After preliminary purification, the membranes were treated according to a purification protocol consisting of three 24 h washings in *aqua ad Iniectabilia* (Braun, Germany) to minimize the residual endotoxin content and remove traces of potentially cytotoxic, pyrogenic organic residues. Membranes had a residual endotoxin content < 20 EU/device, as prescribed for fully implantable medical devices.

4.2. Endotoxin measurement

Biosynthesized cellulose membrane (20 cm^2) was cut using a depyrogenated set of scissors or a scalpel, making sure to cut the sample on a depyrogenated stainless steel (SS) surface. The samples were transferred into a Whirlpak Bag or apyrogenic glassware (Erlenmeyer flask 250 ml) using depyrogenated forceps. 40 mL of LRW (LAL Reagent Water) were added to the Whirlpak Bag or apyrogenic glassware (Erlenmeyer flask 250 ml) and the container was placed into an incubator (36–38 °C) or water bath shaker for at least 15 min. Shaking the initial sample inside of the incubator or water bath shaker. A portion of the extract was transferred into a depyrogenated conical tube. 25 μl aliquots of the endotoxin extract fluid were transferred into each of the four wells of the PTS cartridge, ensuring no bubbles were present in the well at the beginning of the assay.

4.3. Mechanical characterization of the cellulose membrane

Membranes were characterized according to ISO 527-3 (Determination of tensile properties) using a uniaxial testing tool (Hounsfield H5KT) using ASTM D638.1 dumbbell shaped samples. The testing speed was set to 50 mm/min. The variables measured were strength (stress at the first local maximum during the test), strain at strength (strain at which the strength is reached), stress at break (stress at which the specimen breaks) and strain at break, (strain at which the break occurs).

4.4. Membrane preparation

The membranes were carefully placed into the plastic blister with the non-structured side facing upwards, in order to be ready for use upon opening of the container. Always operating in sterile conditions, the container was placed into a second blister and sealed. After sealing, the membranes were steam sterilized (121 °C, 15 min).

4.5. Experimental animals

The animals used in this study were adult female minipigs weighing approximately 40 kg at the time of implantation. The entire study was performed in the framework of the EU directive 2010/63, the German animal protection law and the animal experimentation regulation (TschVersV) after permission granted by license G 0116/17 issued by the LaGeSo Berlin. Details in the *Surgical preparation, coated device implantation and postsurgical monitoring*, *Housing and husbandry* and *Animal Welfare* sections of Materials and Methods are taken from the Standard Operating Procedures of the Animal Facility (FEM) of the Charité-Universitätsmedizin Berlin and reported as requested by the ARRIVE Guidelines.

4.6. Animal study design

Sixteen (n = 16) animals were included in the study. In order to reduce the number of animals and considering the local effects of the formation of the fibrotic tissue, each animal received one cellulose coated pacemaker (PMC), one native pacemaker (BI). Equivalent anatomical sites were chosen for the implantation of the test and control specimens, with the test implant site contralateral to the control implant site, thereby minimizing the number of animals as each animal served as its own control.

The study was undertaken in four consecutive steps: acclimatization of the animals in the animal facility, simultaneous implantation of the BI, PMC, monitoring (observation, physical inspection, blood sampling), followed by explant and histopathological analysis.

A first group of eight (n = 8) subjects was followed up for a period of 3 months, while the remaining eight (n = 8) subjects were followed up for 12 months. One animal was sacrificed at 4 months after implantation due to a persistent lameness and back pain after socialisation trial with another animal from the study. Section of the animal showed no indication that the clinical symptoms were caused by the implantation or the tested material.

4.7. Housing, husbandry and animal welfare

On arrival, all animals were examined and were given an acclimatization period of at least 7 days prior to the experiment. The animals were then kept in groups of 2–4 per stable compartment, which each provided a shelter for retraction, automatic water drinker and entertainment toys. Animals were fed twice per day (morning and evening) with dry pelleted food (15–20 g/kg/day per animal). The room temperature was constantly at 20 ± 2 °C at a relative air humidity of around 55 ± 10%. The artificial light was turned on from 8:00 a.m. until about 6:00 p.m., but roof windows ensured sufficient natural daylight intake. Prior to the experiment, the general condition of each animal was monitored by the animal care takers twice a day and at least two times a week by a veterinarian. Once a week each minipig was allured with food onto a scale to determine its current weight.

4.8. Surgical preparation, coated device implantation and postsurgical monitoring

The animals were fasted for at least 12 h before surgery. In order to reduce stress and to sedate the animals prior to induction of anaesthesia, they were pre-medicated in the stable, with an intra-muscular injection of 25 mg/kg Ketamin, 3,5 mg/kg Xylazin, 3 mg/kg Azaperon and 0,25 ml/10 kg Atropinsulfate. After loss of righting reflex, animals were transported to the animal operation theatre, where oxygen was applied over a mask and a venous catheter was placed in the ear-vein. Propofol was applied (bolus 1–2 mg/kg, intra-venous) to achieve relaxation and swallow-reflex diminishment sufficient for intubation.

After intubation anaesthesia was deepened giving a further propofol bolus to stop spontaneous breathing. Furthermore, a Fentanyl bolus was applied for analgesia. Anaesthesia was maintained by positive pressure respiration of Isoflurane (1,2% - 1,8%) in pure oxygen. For intraoperative analgesia Fentanyl was applied continuously with 1–4 μg/kg/h. During the whole surgical procedure, infusion solution was applied continuously. The operation area was washed and shaved, and a urine catheter was placed. During the entire preparation procedure, the status of the animal was monitored using pulse-oximetry, ECG, non-invasive blood pressure monitoring and capnometry.

The ventral neck, shoulder and chest of the pig were prepped and draped surgically using 10% povidone-iodine and 80% alcohol rinse. Sterile surgical drapes were used to entirely cover the animal while keeping the shoulder/chest area adequately exposed.

Standard sterile operative techniques (equivalent to those for human implantation) were used, including change of gloves and instruments at each implant placement, ensuring haemostasis before implant insertion, minimizing implant handling, and avoiding contact of the implant with the animal skin.

After skin incision and preparation of a subcutaneous device pocket, an active fixation bipolar pacemaker lead (Medtronic, USA) was implanted transvenously via the internal jugular vein and placed in the right atrium under fluoroscopic guidance. The lead was connected to a single chamber pacemaker device (Medtronic, USA). The BC membrane was transferred to the operating table inside its packaging, preserving the orientation with the unstructured side of the membrane facing upwards. The generator was placed above the coiled-up leads, in the same fashion to what is commonly performed according to implantation guidelines. The pacemaker and the proximal part of the leads were wrapped by the cellulose membrane in a manner that the device and the lead were completely covered by the cellulose membrane.

The cellulose covered device was then inserted into the subcutaneous pocket on the left and right lateral chest wall of the animal. The surgical wound was closed in two layers: absorbable sutures, 3–0 Vicryl plus and 4-0 undyed Monocryl (Ethicon, USA) were used for the sub-cutaneous and intra-cutaneous sutures, respectively. OpSite spray (Smith&Nephew, USA) was applied over the operative wounds to reduce the risk of exogenous contamination of the wound. The pacemaker systems were left *in situ* for a time period of 3 or 12 months. For postoperative pain relief Buprenorphin was injected 0.1 mg/kg i.m. and a fentanyl patch was applied releasing fentanyl for three consecutive days.

During the entire experimental procedure until the animal was fully awake, the animal was monitored using pulse-oximetry, ECG, invasive arterial blood pressure measurement, capnometry, respiration counter, arterial and venous blood gas analyses. Based on those parameters, anaesthesia was adjusted.

Once the surgical procedure was completed, the protective wound-draping was applied. After regaining consciousness (swallowing, spontaneous movement etc.) the animal was brought back into its stable and monitored hourly for the first 2–4 h after the surgery.

4.9. Retrieval and histopathological analysis of the devices

Macroscopic and histological examinations were performed to evaluate the biological response to the implanted BIs and PMCs. PMCs findings were compared to that observed in the control PMs. Immediately after sacrifice, the animals underwent a partial necropsy to remove the implants and examine macroscopically the surrounding soft tissues. The PMs were explanted together with the surrounding fibrotic capsule and sufficient unaffected tissue and were examined for any gross anomalies, such as hyperaemia and hemorrhages. The presence, amount and nature of any fluid within the implant cavity or any material adhered to the BI were recorded. The inner surface of the capsule was inspected at the time of necropsy and after formalin fixation of the samples. Macrophotography was used to document relevant observations. Excised PMs and the surrounding soft tissues were fixed for 72 h in adequate amounts of 10% neutral buffered formalin (Formafix, Switzerland). Briefly, each implant capsule was incised along the midline and the PMs gently removed as a whole, although cutting of the leads, strongly embedded in the surrounding capsular soft tissues, was necessary in some BIs to allow removal of the devices.

The histological sections (3–5 μm thick) were prepared and routinely stained for hematoxylin and eosin (HE) and van Gieson (VG) for the histological examination and collagen quantification respectively. Phospho-Tungstic Acid Hematoxylin (PTAH) special stain was selectively used in some cases to stain fibrin. Immunohistochemical evaluation was also performed to detect ionized calcium binding adaptor molecule 1 (Iba-1/macrophages), CD3 (T-lymphocytes), CD20 (B-lymphocytes) and CD31 (endothelial cells). Detailed information about the antibodies, antigen retrieval and detection methods are provided in Methods Table 1. For Iba1, CD20 and CD31 antibodies Dako autostainer (Dako, Glostrup, Denmark) system was used whereas the Discovery XT autostainer (Ventana Medical System, Inc, Tucson, Arizona, USA) system was used for the CD3 antibody. Briefly, antigen retrieval was performed in all the antibodies using citrate buffer (pH 6) at 98 °C for 20 min or EDTA buffer (pH 9) at 98° for 20 min and CC1 buffer (pH 8.4). Subsequently, endogenous peroxidase activity was quenched with hydrogen peroxidase for 10 min. Primary antibodies were incubated for 1 h followed by secondary antibody application. Different detection kits were used (Methods Table 1). Finally, sections were counterstained with hematoxylin for 40 s and mounted. Pig lymph node served as positive control for Iba1, CD3 and CD20 antibodies and lung tissue was used for CD31. Two negative controls were used, one with omission of the primary antibody and one with an isotype-matched irrelevant antibody.

Methods Table 1
Antibodies and immunohistological methods. Abbreviations: Iba-1, ionized calcium binding adaptor molecule 1; CD, cluster of differentiation; citrate, citrate buffer pretreatment; EDTA, EDTA pretreatment; CC1, cell conditioning 1 pretreatment; mAb, monoclonal antibody; pAb, polyclonal antibody.

Antigen	Antibody (clone)	Source	Dilution	Pre-treatment	Detection
Iba-1	Rabbit pAb (019–19741)	Wako	1:750	Citrate	Envision Rabbit (Dako)
CD3	Mouse mAB (M725401-2)	Dako	1:100	CC1	ChromoMap DAB (Ventana Medical Systems)
CD20	Rabbit pAb (RB-9013-P0)	Thermo Scientific	1:700	n/a	Envision Rabbit (Dako)
CD31	Rabbit pAb (sc-1506)	Santa Cruz	1:1500	EDTA	Envision Rabbit (Dako)

Histopathological features were scored in a blind fashion according to a semi-quantitative scoring system suggested in Annex E of International Standards Organization (ISO) 10993-6-2016, which takes into consideration - among others - the extent of fibrosis/fibrous

capsule, the extent and nature of the associated inflammatory reaction, the presence and extent of degeneration/necrosis and the degree of vascularization. According to these premises, the following histopathological features were evaluated: number of fibroblasts, number of inflammatory cells, presence of multinucleated giant cells, fibrin deposition, synovial metaplasia, neovascularization, hemorrhages, capsular erosion and haemosiderin (Supplementary Table 1). Each category was scored with a number that represented the severity of the histological change: 0 = not present; 1 = mild; 2 = moderate; 3 = severe. A total score representing the severity of biological response to the device was obtained by summing the scores of each histological feature (Table 1). The extent of fibrosis was further analysed using a histomorphometric approach, as detailed in the next paragraph. All HE-stained slides were scanned using a digital slide scanner (NanoZoomerXR C12000, Hamamatsu, Japan) and images were taken using NDP.view2 viewing software (Hamamatsu).

4.10. Image Analysis

Lateral size or projected diameter of the fibers, was calculated from SEM images using the measurement tool of ImageJ.

For the quantitative assessment of the fibrotic tissue thickness, the digital images were imported into ImageJ (National Institute of Health, USA) using the NDPITools plugin [35].

The fibrotic tissue thickness was determined using first the "Freehand line" tool to manually select the fibrotic tissue layer. The selected regions were exported as regions of interest and then the "Measurements" tool of ImageJ was used to obtain the thickness value in cm. The measurement protocol foresaw taking 36 individual thickness measurements per implant analysed. The independent measurements were then averaged in order to obtain the mean fibrotic tissue thickness for each independent position.

Visiopharm software (Visiopharm Integrator System, Version 5.0.4. 1382; Visiopharm, Horsholm, Denmark) was used to label the collagen fibres stained with VG special stain. First, manual annotations were introduced to select the fibrotic capsule and subsequently threshold classification method was applied to label the collagen bands.

4.11. Statistical analysis

Statistical comparison of population means was performed using a paired Student's T-test (after data assessment for Normality) or a non-parametric Paired-sample Wilcoxon Signed Rank test. The effect was quantified on a single scalar parameter (i.e. thickness of fibrotic tissue) measured in two conditions (i.e. test condition with BC protection and control bare implant) in each experimental animal. The total number of measurements is shown in the upper or lower right-hand corner of the presented graphs in Fig. 8. For box plots the size depicts the measured standard error of the mean and the whiskers the standard deviations of the populations.

Appendix A. Supplementary data

Supplementary data to this article can be found online at https://doi.org/10.1016/j.biomaterials.2019.119583.

References

[1] A.J. Greenspon, et al., Timing of the most recent device procedure influences the clinical outcome of lead-associated endocarditis: results of the MEDIC (Multicenter Electrophysiologic Device Infection Cohort), J. Am. Coll. Cardiol. 59 (7) (2012) 681–687.

[2] A. Voigt, S. Saba, The truth is in the details, Circulation 137 (1) (Jan. 2018) 34–37.

[3] M. Brignole, et al., ESC Guidelines on cardiac pacing and cardiac resynchronization therapy: the Task Force on cardiac pacing and resynchronization therapy of the European Society of Cardiology (ESC). Developed in collaboration with the European Heart Rhythm Association (EHRA), Europace 15 (8) (2013) 1070–1118.

[4] J. Byles, "Our Ageing World," in *Geriatric Medicine*, Springer Singapore, Singapore, 2018, pp. 1–13.

[5] R.E. Kirkfeldt, J.B. Johansen, E.A. Nohr, O.D. Jorgensen, J.C. Nielsen, Complications after cardiac implantable electronic device implantations: an analysis of a complete, nationwide cohort in Denmark, Eur. Heart J. 35 (18) (2014) 1186–1194.

[6] J.E. Poole, et al., Complication rates associated with pacemaker or implantable cardioverter-defibrillator generator replacements and upgrade procedures, Circulation 122 (16) (Oct. 2010) 1553–1561.

[7] R. Steckiewicz, E.B. Świętoń, A. Kołodzińska, M. Bogdańska, Fus, P. Solarz, Morphometric parameters of cardiac implantable electronic device (CIED) pocket walls observed on device replacement, Folia Morphol. 76 (4) (Dec. 2017) 675–681.

[8] H.R.C. BIEFER, et al., Generator pocket adhesions of cardiac leads: classification and correlation with transvenous lead extraction results, Pacing Clin. Electrophysiol. 36 (9) (Sep. 2013) 1111–1116.

[9] J.M. Anderson, A. Rodriguez, D.T. Chang, Foreign body reaction to biomaterials, Semin. Immunol. 20 (2) (2008) 86–100.

[10] C.I. Nichols, J.G. Vose, S. Mittal, Incidence and costs related to lead damage occurring within the first year after a cardiac implantable electronic device replacement procedure, J. Am. Heart Assoc. 5 (2) (2016) 1–9.

[11] P.P. Borek, B.L. Wilkoff, Pacemaker and ICD leads: strategies for long-term management, J. Interv. Card Electrophysiol. 23 (1) (Oct. 2008) 59–72.

[12] D. Klug, et al., Risk factors related to infections of implanted pacemakers and cardioverter-defibrillators, Circulation 116 (12) (Sep. 2007) 1349–1355.

[13] W.K. Czaja, D.J. Young, M. Kawecki, R.M. Brown, The future prospects of microbial cellulose in biomedical applications, Biomacromolecules 8 (1) (Jan. 2007) 1–12.

[14] D. Klemm, et al., Nanocelluloses: a new family of nature-based materials, Angew. Chemie Int. Ed. (2011).

[15] Q. Wei, et al., Protein-resistant surfaces protein interactions with polymer coatings and biomaterials, Angew. Chem. Int. Ed. 53 (2014) 8004–8031 July.

[16] C.J. Bettinger, R. Langer, J.T. Borenstein, Engineering substrate topography at the micro- and nanoscale to control cell function, Angew. Chem. Int. Ed. 48 (30) (Jul. 2009) 5406–5415.

[17] A. Ferrari, M. Cecchini, Cells on patterns, in: A. del Campo, E. Arzt (Eds.), Generating Micro- and Nanopatterns on Polymeric Materials, vol. 10, Wiley-VCH Verlag GmbH & Co. KGaA, Weinheim, Germany, 2011.

[18] A.F. Von Recum, T.G. Van Kooten, The influence of micro-topography on cellular response and the implications for silicone implants, J. Biomater. Sci. Polym. Ed. 7 (2) (Jan. 1996) 181–198.

[19] J. Allen, J. Ryu, A. Maggi, B. Flores, J.R. Greer, T. Desai, Tunable microfibers suppress fibrotic encapsulation via inhibition of TGFβ signaling, Tissue Eng. Part A 22 (1–2) (2016) 142–150, https://doi.org/10.1089/ten.tea.2015.0087.

[20] R. You, X. Li, Y. Liu, G. Liu, S. Lu, M. Li, Response of filopodia and lamellipodia to surface topography on micropatterned silk fibroin films, J. Biomed. Mater. Res. Part A 102 (Feb. 2014) 12 n/a-n/a.

[21] A. Ferrari, et al., Nanotopographic control of neuronal polarity, Nano Lett. 11 (2) (2011) 505–511.

[22] F. Robotti, et al., The influence of surface micro-structure on endothelialization under supraphysiological wall shear stress, Biomaterials 35 (30) (Oct. 2014) 8479–8486.

[23] D. Franco, et al., Control of initial endothelial spreading by topographic activation of focal adhesion kinase, Soft Matter 7 (16) (Aug. 2011) 7313.

[24] F. Robotti, et al., A micron-scale surface topography design reducing cell adhesion to implanted materials, Sci. Rep. 8 (1) (Dec. 2018) 10887.

[25] S. Bottan, et al., Surface-structured bacterial cellulose with guided assembly-based biolithography (GAB), ACS Nano 9 (1) (2015) 206–219.

[26] F. Bassetto, C. Scarpa, E. Caccialanza, M.C. Montesco, P. Magnani, Histological features of periprosthetic mammary capsules: silicone vs. Polyurethane, Aesthet. Plast. Surg. 34 (4) (Aug. 2010) 481–485.

[27] P. J. Bradshaw, P. Stobie, M. W. Knuiman, T. G. Briffa, and M. S. T. Hobbs, "Trends in the Incidence and Prevalence of Cardiac Pacemaker Insertions in an Ageing Population".

[28] J.B. Johansen, O.D. Jorgensen, M. Moller, P. Arnsbo, P.T. Mortensen, J.C. Nielsen, Infection after pacemaker implantation: infection rates and risk factors associated with infection in a population-based cohort study of 46299 consecutive patients, Eur. Heart J. 32 (8) (Apr. 2011) 991–998.

[29] K.G. Tarakji, et al., Worldwide randomized antibiotic EnveloPe infection PrevenTion trial (WRAP-IT), Am. Heart J. (180) (2016) 18–21, https://doi.org/10.1016/j.ahj.2016.06.010.

[30] M.A. Padalino, et al., Early and mid-term clinical experience with extracellular matrix scaffold for congenital cardiac and vascular reconstructive surgery: a multicentric Italian study, Interact. Cardiovasc. Thorac. Surg. 21 (1) (Jul. 2015) 40–49.

[31] M. Trochsler, G.J. Maddern, Adhesion barriers for abdominal surgery: a sticky problem, Lancet (Lond., Engl.) 383 (9911) (Jan. 2014) 8–10.

[32] H. Güngör, C. Zencir, T. Tekten, Percutaneous extraction of implantable cardioverter defibrillator electrode with mechanical dilator sheath, Int. J. Cardiovasc. Acad. 2 (1) (Mar. 2016) 38–39.

[33] K.A. Polyzos, A.A. Konstantelias, M.E. Falagas, Risk factors for cardiac implantable electronic device infection: a systematic review and meta-analysis, Europace 17 (5) (2015) 767–777.

[34] D.F. Williams, On the mechanisms of biocompatibility, Biomaterials 29 (20) (Jul. 2008) 2941–2953.

[35] C. Deroulers, D. Ameisen, M. Badoual, C. Gerin, A. Granier, M. Lartaud, Analyzing huge pathology images with open source software, Diagn. Pathol. 8 (1) (Dec. 2013) 779.